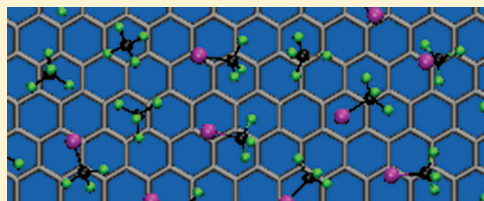


Characterization of $\text{CF}_4/\text{CF}_3\text{Br}$ Binary Mixture Adsorption on Hydrophobic/Hydrophilic Surfaces via Atomistic MD Simulation

Gary M. Leuty* and Mesfin Tsige*

Department of Polymer Science, The University of Akron, Akron, Ohio 44325-3909, United States

ABSTRACT: Molecular dynamics simulations of multilayer adsorption of binary mixtures of two tetrasubstituted halomethanes (CF_4 and CF_3Br) on two very different substrates (graphite vs hydroxylated SiO_2) were performed for three different bulk compositions (40%, 50%, and 60% CF_4) and over a range of temperatures from 80 to 200 K. The goal of these simulations was to investigate in depth how these factors affect film structure, layer composition, lateral arrangement, and molecular orientation in the first adsorbed layer on each substrate. In line with a previous study of single-component adsorption on these surfaces, mixtures adsorbed on the hydroxylated SiO_2 surface show stable number density profiles that are largely independent of temperature, up to 160 K. This level of stability is essentially absent in the case of adsorption on graphite, which show densities and surface populations that are largely dependent on overall film composition, molecular orientation, and adsorbate–substrate interactions, in addition to system temperature. Further, the composition of the first adsorbed layer at each solid surface appears to be influenced by the choice of substrate, with CF_3Br the majority component at the graphite surface for all compositions and temperatures, while the first adsorbed layer on hydroxylated SiO_2 more clearly mirrors the overall film composition at temperatures below 160 K.



INTRODUCTION

For a number of years, studies of adsorption of small molecules on surfaces have been used as a method of studying the fundamental interactions and phase transitions of systems of lower dimensions in order to describe surface structures and characterize transitions. The importance of investigating low-dimensional systems—from two-dimensional phases on surfaces and at interfaces^{1–9} to one-dimensional or quasi-one-dimensional matter such as regions on, inside, or in the interstitial spaces between single-walled carbon nanotubes—cannot be underestimated for materials science, owing to the large number of applications generated. Questions of adsorption in these low-dimensional systems—especially in the case of the aforementioned carbon nanotubes, which has excited a sizable amount of experimental^{10–12} and theoretical or simulation^{13–16} study—seem particularly well-suited to computational simulation, where processes occurring at the smallest time and length scales can be probed efficiently and to a suitable degree of detail.

In recent years, concern over the possibility of anthropogenic climate change caused by radiative forcing from CO_2 and other “greenhouse gases”, such as the fluorocarbons dealt with in this study, have also reintroduced adsorption processes as important practical means of reducing release or eliminating remnants of these compounds.¹⁷ Pressure swing adsorption (PSA) and related adsorption methods^{18–20} have been promoted as possibly offering convenient approaches for removal or reclamation of postcombustion CO_2 and other gases related to climate concerns. Such methods also bear the ability to capture precombustion gases from cleaner-burning fuel streams, possibly decreasing emissions of harmful gases while simultaneously improving

combustion efficiency and energy extraction. Methods have even been considered that rely on adsorption on or inside carbon nanotubes²¹ as a means of eliminating or reducing tetrafluoromethane (CF_4) emission.

Of pivotal importance to the fundamental science of adsorption and the feasibility of any applied use therein is the interaction between an adsorbent surface and the adsorbate species. In this study, we have attempted to extend our earlier molecular dynamics (MD) simulation study²² (hereafter referred to as Paper I) of adsorption of pure halomethane films on the surfaces of graphite and hydroxylated SiO_2 to view the behavior of binary mixtures of two of the halomethane compounds (CF_4 and CF_3Br) to study not only the interactions between the adsorbate species and the substrates as a function of temperature but also the interactions between CF_4 , an essentially spherical nonpolar species, and CF_3Br , a polar molecule with pronounced asymmetry due to the replacement of a fluorine atom with a much larger bromine, by examining the effect of changing the composition of the mixtures to reflect equal and unequal contributions of each component. The temperature at which simulations take place is also expected to have a significant effect on adsorption characteristics; thus, we have simulated the adsorption of these binary mixtures over a range of temperatures from 80 to 200 K to examine adsorption behavior as each component traverses its solid–liquid and liquid–vapor phase transitions.

Received: June 17, 2011

Revised: September 12, 2011

Published: September 28, 2011

Molecular dynamics simulation is well suited to this type of problem for the resolution it offers at very small time and length scales. The molecular- and atomic-level descriptions of these adsorption processes have provided us with an in-depth characterization of structure, organization, and orientation that are very difficult to obtain experimentally but are the underpinning of the macroscopic qualities that make adsorption useful for the aforementioned applications and more.

In the past, numerous studies of adsorption of single-component films^{23–28} on substrates such as graphite have been made to elucidate molecular arrangements and orientation as a means of delving into their complex 2D phase behavior and to discuss the nature of phase transitions occurring in 2D or quasi-2D matter. The addition of a second component to such films, as is the case in the following study, adds an entirely new layer of complexity to the problem of simple adsorption on surfaces, as the interplay between adsorbate–substrate interactions for each component, as well as adsorbate–adsorbate interactions between components, changes the landscape considerably and invites new questions. A recent investigation by Thomas et al.²⁹ into the competition between CF₄ molecules and CF₃Cl monolayers at a graphite surface highlights this complexity and raises further questions about the precise factors that control this competition for adsorption and how they can be altered.

In light of such rich behavior at the base of studies of binary mixture adsorption, we have attempted to present, in great detail, a thorough investigation of how factors such as overall film composition, temperature, and substrate–adsorbate interactions affect structural characteristics of the film as a whole as well as molecular-level structural arrangement and orientation of the first adsorbed layer. While adsorption of the compounds studied here has some precedence for study from both simulation and experiment, data for adsorption of either fluoromethane compound appears to be significantly lacking, and little in the way of clear experimental data currently exists regarding the adsorption of mixtures of such compounds on the substrates. Our goal, then, is to present several different perspectives on adsorption behavior in the hopes that such detail may reinvigorate research, both theoretical and experimental, into investigations of the properties of mixtures such as these on surfaces of varied composition, in order to explore many new possible areas of interest.

METHODOLOGY

Binary mixture films used in the simulations in this study were composed of a total of 1000 molecules in all cases, with three different film compositions considered: 40% CF₄ (400 CF₄ molecules vs 600 CF₃Br molecules), 50% CF₄, and 60% CF₄. The adsorbents used in the simulations are identical in composition and construction to those used in Paper I for the study of adsorption of pure halomethane films, owing to the desire to make the studies as comparable as possible. Both the freezing of the positions of the carbon atoms in the graphite substrate and the vibrational freedom allowed to the surface hydroxyl groups on the SiO₂ surface used in Paper I were reproduced for this study.

The set of potential energy functions and parameters used to model intermolecular and intramolecular atomic interactions were derived from the OPLS-AA (optimized potentials for liquid simulations—all-atom) force field developed by Jorgensen and Watkins;³⁰ the specific values for the interaction parameters

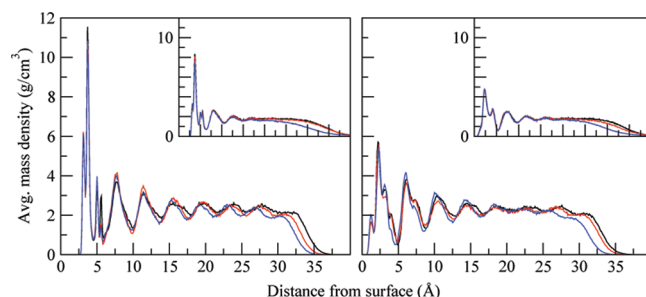


Figure 1. Comparison of average mass density for binary mixture films at 80 K adsorbed on graphite (left) and SiO₂ (right). Film bulk compositions are 40% CF₄ (black), 50% CF₄ (red), and 60% CF₄ (blue). Inset: average mass density at 200 K.

and the functional forms are also fully detailed in Paper I and will not be reproduced here.

Simulations were performed largely over a range of temperatures from 80 to 200 K, in increments of 10 K for simulations at or below 100 K, 20 K for simulations between 100 and 160 K, and 40 K for simulations above 160 K (a single case at 200 K). All simulations were performed using the LAMMPS molecular dynamics package,³¹ utilizing velocity–Verlet integration with a time step of 1 fs. All adsorption simulations were preceded by equilibration runs in the isothermal–isobaric (NPT) ensemble and with periodic boundary conditions enforced in all directions for binary mixtures without substrates, to create an equilibrium bulk adsorbate. Equilibration runs lasted between 3 and 5 ns in length, which was enough time to allow the bulk to reach the proper state. The system temperature was maintained above the melting points of both components of the film by use of Nosé–Hoover thermostat; a similar barostat was applied to manage the system pressure.

The adsorption phase of the simulations began with the film placed 5 Å above the surface of the substrate of choice, for the same reasons used in Paper I. Simulations in this phase were carried out in the canonical (NVT) ensemble, with temperature controlled via Nosé–Hoover thermostat. The cutoff for van der Waals interactions was set at 12 Å; simulation subsequent to Paper I revealed minimal difference in results using this cutoff or a larger 15 Å cutoff. Equilibration in this phase, with the film and substrate together, was achieved in roughly 5–6 ns for the majority of cases; at low temperatures, dynamics often dictated the use of a longer interval for equilibration, in some cases 15 ns or more. All systems were monitored to ensure proper equilibration, and data for analysis was recorded every 1 ps over a further 1.5 ns of simulation time.

RESULTS AND DISCUSSION

Characterization at Interfaces. We begin this study, as with Paper I, by examining the average mass density of the adsorbed films as a function of the distance from the substrate surface along the normal to the surface (in this case, the z-axis). This was done by partitioning the simulation space into bins along the z-axis and calculating the mass density within each bin using the positions and masses of each atom. It is readily apparent that performing this calculation in the manner prescribed makes the result of the average density calculation partially dependent on the choice of bin width; in the following, the width of the bins has been fixed at

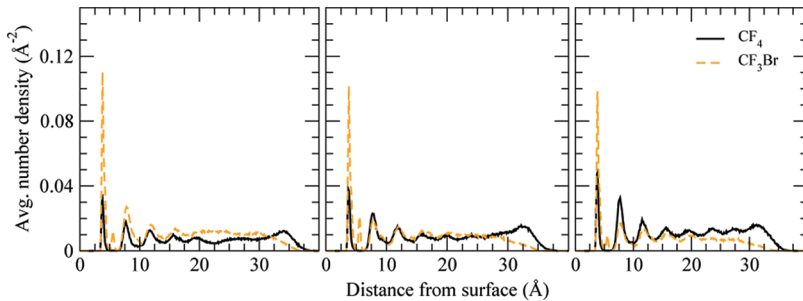


Figure 2. Average number density of adsorbed binary mixtures on graphite at 100 K, classified by adsorbate species, as a function of distance from the substrate surface. Bulk film compositions are 40% CF_4 (left), 50% CF_4 (center), and 60% CF_4 (right).

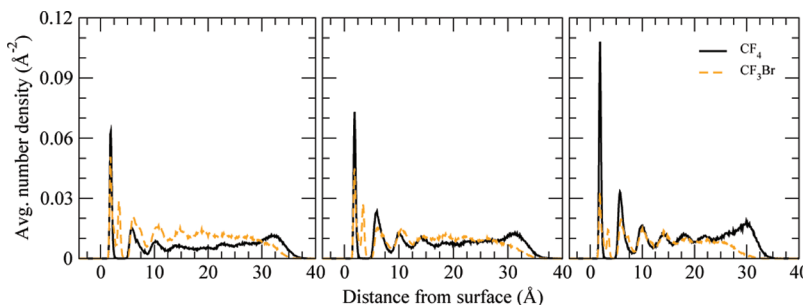


Figure 3. Average number density of adsorbed binary mixtures on hydroxylated SiO_2 at 100 K, classified by adsorbate species, as a function of distance from the substrate surface. Bulk film compositions are 40% CF_4 (left), 50% CF_4 (center), and 60% CF_4 (right).

0.1 Å in an attempt to preserve finer features of the density profile. The result of this calculation is plotted in Figure 1.

In Figure 1, one of the first conclusions drawn comes from the presence of an oscillatory profile for films adsorbed on both substrates, pointing (as in Paper I) to the presence of distinct layers of adsorbed molecules. At the first layer, nearest the surface, sharp variations in mass density are produced by preferences for specific orientations for each of the component molecules at the substrate surface (this facet is treated in depth in the next section). Beyond this first layer, at low temperatures, distinct oscillations persist to a depth of 25–30 Å for films on graphite, giving rise to several distinct layers, while such distinct oscillations on the hydroxylated SiO_2 surface seem to remain to depths of 20–25 Å, with fewer clear layers. As temperature increases and molecules become more mobile, the oscillations in the bulk liquid give way to a more constant density profile with an average mass density comparable to the liquid-phase density of the components, combined in the prescribed ratios.

It is also notable that fluctuations are comparable across each film composition up to the introduction of the film–vapor interface. At the interface, Figure 1 shows that the position of the interface is slightly altered by the composition of the bulk, reflecting the differences in density of the components involved. System temperature, on the other hand, has a dramatic effect on the width of the liquid–vapor interfaces for each case. At 80 K, the interfaces for each film composition are comparably sharp and the widths narrow, whereas at 200 K and beyond, at temperatures near or above the bulk boiling points of both components (145.16 K for CF_4 ³² and 215.29 K for CF_3Br ³³), the decrease in density signaling the liquid–vapor interface becomes extremely broad; beyond surface layering induced by interactions with the substrate, the liquid phase of the mixture gives way quickly to the vapor phase at these temperatures.

While the average mass density provides information on essential variations in surface layering and interfacial behavior, to view information on how each species arranges with respect to the bulk and the interfaces, an overall average number density was calculated in similar fashion to the average mass density in Figure 1, but with regard for the numbers of each component present in the film. After partitioning the simulation space into bins along the normal direction (z -axis), the position of a given molecule was taken as the location of the central carbon atom of the molecule, and the number of molecules of each species within a bin was counted and divided by the bin volume. Figure 2 and Figure 3 show the results of this calculation for a representative temperature of 100 K. This temperature was assumed to be one in which both species were in the liquid phase or moving to the liquid phase and thus should offer appropriate insight into the mixing characteristics of the films next to the surface.

Near the surfaces, the packing of molecules changes dramatically, both in number and in composition. In the case of adsorption on graphite, polar CF_3Br dominates the population at the substrate interface. From the figure, it can be seen that the population of CF_3Br in the first layer above the surface decreases when the fraction of CF_3Br in the overall film decreases, and the population of CF_4 is seen to increase at the same time, as the amount of CF_3Br decreases. If the number density of each component in the first layer were seen to behave like the bulk composition of the film, this result would be expected. However, it is clear that even in the film composed of 60% CF_4 , the amount of CF_3Br at the surface far surpasses the amount of CF_4 , suggesting a stronger interaction between CF_3Br and the graphite surface. Also of note in Figure 2 are the small secondary peaks in the number density of the first layer beyond the large, narrow first peak. We suggest that this is also a first-layer peak, reflecting differences in orientation of

CF_3Br molecules that are not possible with CF_4 molecules. Both the nature of this change in orientation and the nature of the interaction that appears to prefer CF_3Br at the graphite substrate surface will be treated in depth in the next section.

The number density of CF_3Br on hydroxylated SiO_2 in Figure 3 can also be seen to exhibit a two-peak structure, with a secondary peak of both greater amplitude and larger width than was the case for adsorption on graphite. When taking this secondary peak into account, the total number of molecules adsorbed on the hydroxylated SiO_2 surface shows much different behavior than the films on graphite. At low concentrations of CF_4 (high CF_3Br), the total CF_3Br number density from the first two peaks shows that CF_3Br is the preferred adsorbate at the surface. As the amount of CF_4 in the overall film increases, however, the number density of CF_3Br is seen to decrease, while the contribution from CF_4 grows. This becomes a pronounced preference for CF_4 at the substrate surface when the overall film composition reaches 60% CF_4 , suggesting that in the case of adsorption on hydroxylated SiO_2 , the primary factor influencing the composition of the first layer is the composition of the overall film, and neither component appears to be preferentially selected, as was the case for adsorption on graphite. This, too, can be influenced by the orientation of the molecules and will be expanded upon in the next section.

One feature of Figure 2 and Figure 3 for all film compositions and at each temperature studied was the low population or exclusion of CF_3Br at the liquid–vapor interface. The preference for one component of a mixture at a liquid–vapor interface is initiated by an appreciable difference in the surface tension of the components; the component with the lower surface tension is able to form a liquid–vapor interface with less of a penalty to the system energy and is thus preferred. In this case, the presence of pure CF_4 at the liquid–vapor interface implies that the surface tension of CF_4 is sufficiently less than that of CF_3Br that the liquid–vapor interface forms to the exclusion of CF_3Br . To test this, separate simulations were performed on free-standing films of pure CF_4 and pure CF_3Br allowed to equilibrate over very long time scales (10–50 ns). Surface tension calculations, the details of which can be found in a previous article³⁴ and include tail corrections, were performed and were monitored throughout the equilibration procedure. The results of the surface tension calculation at equilibrium for four temperatures (105, 110, 115, and 120 K) are shown in Figure 4.

These surface tension calculations clearly show CF_4 as having the lower surface tension at each temperature studied, confirming the findings of the number density calculations; the difference between the two is appreciable enough to indicate why CF_3Br is essentially excluded completely at the interface. It is somewhat difficult to find sources for comparison in experimental literature for surface tension values at such low temperatures; nevertheless, we have found our simulation values to be in good agreement with surface tension data obtained from experiment for CF_4 .³⁵ In the case of CF_3Br , Rathjen and Straub³⁶ describe an empirically derived fitted curve for the surface tension, from which parameters were obtained for CF_3Br . From this, it is possible to extrapolate surface tension values at the temperatures seen in Figure 4. While values from the experimental fit appear to be comparable to but lower than those derived from our simulations, both share the quality of being significantly higher than the expected surface tension of CF_4 .

Between the solid–liquid interface at the substrate—where density oscillations imposed by the substrate interactions suggest

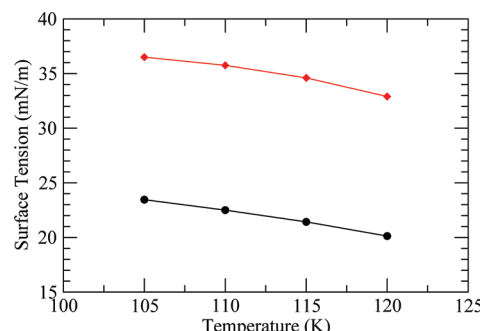


Figure 4. Surface tension of CF_4 (black line) and CF_3Br (red line) as a function of simulation temperature over a range of temperatures assumed to lie within the liquid phase of either component. Error bars are within width of symbols and have been suppressed.

differences in binding potential between substrate types—and the liquid–vapor interface in the region exposed to vacuum, where surface tension dominates the expression of one species, lies the bulk liquid phase of the binary mixtures. Figures 2 and 3 show that the composition of this region, while heavily dependent on behavior at the interfaces, retains an essentially uniform distribution in each case. Although Figures 2 and 3 present the number density at one temperature, this characteristic has been noted for the other temperatures simulated as well.

Both the average mass density and the per-molecule number density (in the case of CF_3Br) show a multiple-peak structure near the surface. In the case of average mass density, it is not clear from Figure 1 whether the pair of split peaks near the graphite surface is indicative of nuanced orientation of a single layer or offset positions of two different layers; for films on hydroxylated SiO_2 , the structure seems more clearly a single layer of molecules at the substrate surface, but with multiple peaks. Figures 2 and 3 suggest that the second density peaks are closely related to the primary peaks and appear only as a result of the polar component. Thus, it seems most likely that a portion of the CF_3Br molecules in the first adsorbed layer have adopted a different orientation relative to the majority, placing a very noticeable portion of the first layer slightly further from the substrate surface.

A more objective measure of the surface-adjacent population can be taken from the average number of molecules in the first layer per unit surface area (henceforth referred to as the molecule number per unit surface area, or MPSA). This can be calculated by integration of the number density over the region in the z -direction corresponding to the first-layer region, or by simple counting of first-layer molecules. This measure can be used as a metric for comparison between substrates having different surface areas (although, in our simulations, the surface area of the graphite substrate is only 0.269% larger than the SiO_2 substrate, at 2767.16 \AA^2 for the graphite substrate vs 2759.75 \AA^2 for the SiO_2). The results of this calculation, comparing the total number of molecules per unit surface area for each substrate, bulk film composition and temperature, are shown in Figure 5.

Evident from Figure 5 is that, similar to in Paper I, the total number of molecules per unit surface area for films adsorbed on SiO_2 is larger than it is in the case of films adsorbed on graphite, regardless of film composition or simulation temperature. Below 160 K, the first-layer MPSA on SiO_2 is essentially constant (0.048 \AA^{-2}), decreasing only above 160 K—to 0.046 \AA^{-2} for the film with 40% CF_4 and 0.047 \AA^{-2} for the films with 50% CF_4 and 60% CF_4 . Conversely, the MPSA of first-layer molecules on graphite

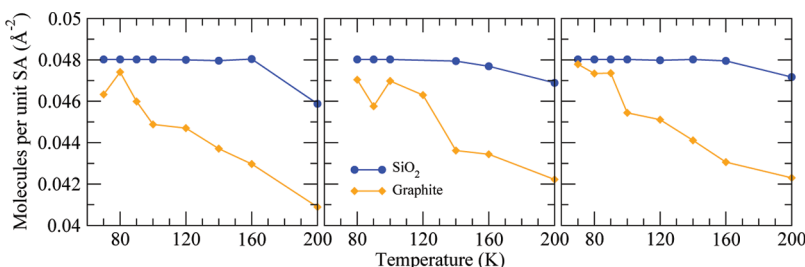


Figure 5. Number of molecules adsorbed on the substrate surface per unit surface area for films of the following composition: 40% CF₄ (left), 50% CF₄ (center), and 60% CF₄ (right). Error bars are within width of symbols and have been suppressed.

fluctuates much more and shows a general decreasing trend as temperature is increased. Below 90 K, the first-layer MPSA on graphite for each film composition is comparable to the corresponding film composition on SiO₂, with films of all three film compositions reaching their maximum values in this range—0.047 Å⁻² for 40% CF₄ and 50% CF₄, and slightly under 0.048 Å⁻² for 60% CF₄. There does not appear to be a specific point at which the MPSA of films on graphite shows a sudden decrease, suggesting perhaps that the loss of molecules from the first layer is essentially continuous as a function of temperature. Regardless of film composition, at the high end of our simulation temperature range, films adsorbed on graphite do appear to have lost a significantly greater number of molecules from the first layer (molecule number per unit surface area—0.041 Å⁻² for 40% CF₄, slightly above 0.042 Å⁻² for 50% and 60% CF₄).

In Paper I, we were also able to determine the number of molecules adsorbed at the surface per unit surface area for films of pure CF₄ and CF₃Br. For films adsorbed on graphite at temperatures below 100 K, we calculated 0.055 molecules of CF₄ per Å², while we found 0.044 molecules per Å² for films of pure CF₃Br on graphite. Both pure films show temperature dependence for the number of adsorbed molecules per unit surface area, dropping roughly 12% for films of CF₄ and 10% for films of CF₃Br, which is roughly in line with the decreasing number of adsorbed molecules per unit surface area seen in mixtures adsorbed on graphite. As such, in the case of the binary mixture of CF₄ and CF₃Br, the number of adsorbed molecules per unit surface area being between the same measurement for pure halomethane films and decreasing similarly suggests that the number of molecules adsorbed on the surface of the graphite is not affected by the mixing of polar and nonpolar compounds, with the behavior akin to the average of noninteracting independent species.

For films of pure CF₄ and CF₃Br on hydroxylated SiO₂, the situation was slightly altered. In comparison with films adsorbed on graphite, we noticed that there were fewer CF₄ molecules per unit surface area on SiO₂ (0.048 Å⁻²) than on graphite, but that the situation was reversed for polar molecules such as CF₃Br, which showed a slightly increased population on SiO₂ (0.048 Å⁻²). Not only does this mean that films of pure CF₄ and CF₃Br separately show the same density of molecules in the first layer of the SiO₂ substrate (possibly suggesting similar affinity for the substrate surface), but also that this result is identical to the total number of molecules per surface area of the CF₄/CF₃Br mixture on the same substrate, suggesting that this may reflect the extent of the carrying capacity for the hydroxylated SiO₂ surface. Further, pure films on the SiO₂ substrate showed very little dependence on temperature (<5% difference over the temperature range studied), which is in line with the trend seen in

Figure 5, where there is essentially no change in the number of adsorbed molecules per unit surface area until the temperature exceeds 160 K, at which point the number per unit surface area decreases, but only by 4–5%. Thus, it appears that the number of molecules able to adsorb onto the surface of the SiO₂ substrate is independent of the choice of adsorbate molecule, even showing no difference when adsorbates of different character are applied together.

The total number of molecules adsorbed on the substrate surface can assist in inferring certain characteristics of how temperature affects the substrate–adsorbate interaction and the amount of molecules the surface can easily accommodate, but the information from this calculation is incomplete in regards to composition of this first adsorbed layer, especially in terms of the composition of the first layer compared to the composition of the bulk film. In the absence of a priori assumptions about interactions between graphite, an atomically flat surface, and fluorine or organofluorine compounds, it might be reasonable to assume that graphite acts ambivalently toward the halomethanes simulated here in the temperature range used, presenting a first adsorbed layer whose population mirrors the bulk composition. This would, however, directly contradict the findings shown in Figure 2, where it was shown that CF₃Br is preferred at the graphite surface. In the case of films on SiO₂, the presence of surface hydroxyl groups produces a structured surface that complicates assumptions about whether an adsorbate is preferred, and the determination of the number of adsorbed molecules per unit surface area in Figure 3 shows that there is no difference in number density at the surface between CF₄ and CF₃Br. Thus, an explicit determination of the composition of the surface layer is in order. For each film composition, temperature, and substrate type, the fraction of the first adsorbed layer taken by a given species has been calculated and recorded in Figure 6.

In Figure 6 (left), the first layer of the mixed film on graphite presents CF₃Br as the majority component at all temperatures and compositions. As the temperature increases, the fraction of CF₄ present in the surface layer begins to decrease, while the fraction of CF₃Br in the surface layer rises in compensation, suggesting that CF₄ present at low temperatures is displaced by CF₃Br as the temperature rises. At 80 K—below the bulk melting temperature of CF₄ (89.5 K⁸), where decreased translational motion of molecules of either component affords less chance for escape and replacement—we see that at all compositions, the percentage of CF₄ present in the surface layer is less than that of the bulk, suggesting possibly either a preference for the graphite–CF₃Br interaction or a size mismatch between the spherical CF₄ and the aspherical, elongated CF₃Br. Indeed, at 80 K, in each composition studied, the concentration of CF₄ in the surface layer never exceeds 45%, even when the percentage of CF₄ in the bulk

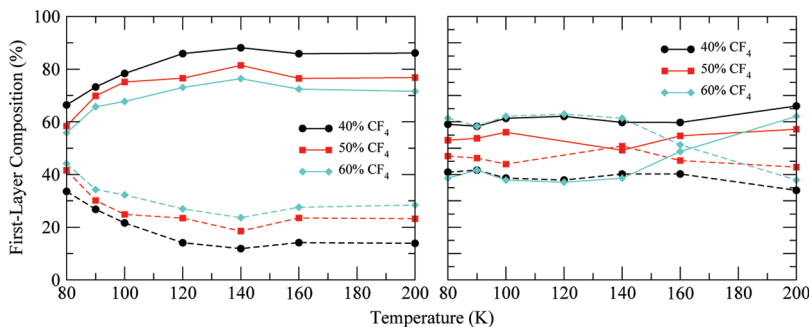


Figure 6. Percent composition of first layer of CF₄/CF₃Br films as a function of simulation temperature for adsorption on graphite (left) and SiO₂ (right). Solid lines represent percentage of CF₃Br present, while dashed lines represent percentage of CF₄ present. Error bars are within width of symbols and have thus been suppressed.

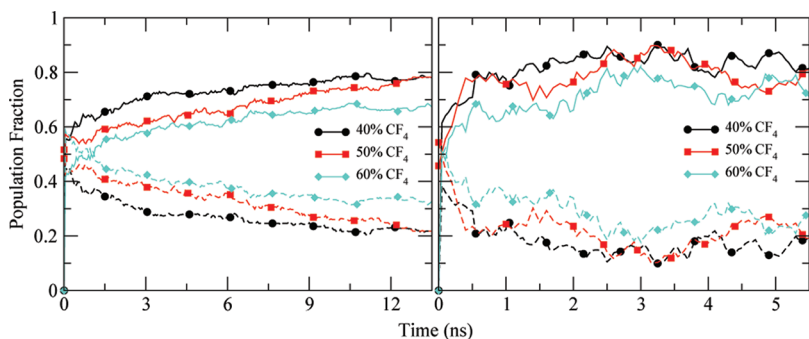


Figure 7. Surface-layer population fractions of CF₄ (dashed curve) and CF₃Br (solid curve) adsorbed on graphite as a function of time for films of differing overall composition at two different temperatures: 100 K (left) and 200 K (right).

reaches 60%. Also notable in this figure is that the change in composition of the overall film elicits a correlated change in the composition of the first layer; it is clear that films with lower CF₄ concentrations overall have markedly lower concentrations of CF₄ in the first layer.

At the right in Figure 6, the percent composition of the first adsorbed layer on SiO₂ shows a different picture. In this case, while fluctuations are prominent in the case of equimolar CF₄ and CF₃Br in the bulk, at temperatures below 140 K, the composition of the first adsorbed layer nearly exactly mirrors the composition of the bulk film, independent of temperature, with the composition of the first layer of the equimolar film fluctuating about equimolar contributions from each component. At 160 K, the concentration of CF₄ in the surface layer decreases (markedly, in the case of 60% CF₄ composition in the bulk film) with a commensurate increase in the CF₃Br concentration, suggesting that the populations of each component of the first layer on SiO₂ remain nearly fixed to this temperature and that, above 160 K, the increased mobility of individual molecules as an effect of rising temperature allows CF₄ the ability to move off the surface, leaving CF₃Br molecules to replace them.

It is reasonable to question whether the temperature-dependent shift in population fraction seen in Figure 6 reflects a surface layer that is stable with respect to number fluctuations as a function of time or one that has yet to reach equilibrium and thus reflects population fractions that are dependent on the window in which the number density calculation is performed. To answer this question, calculations were performed to show the population fraction of each species within the surface layer as a function of time. In the case of molecules adsorbed on graphite, all of the

simulations performed appear to reach some form of equilibrium within the simulation window. This appears to take much more time—roughly 10 ns—for simulations carried out at lower temperatures (100 K and below, Figure 7 left) than it does for simulations performed at higher temperatures (200 K, Figure 7 right), for which equilibration appears to take hold at roughly 2.5 ns.

However, adsorption of molecules on SiO₂ presents a very different view of the dynamics. In Figure 8, we see systems at the same temperatures shown in Figure 7, but on the SiO₂ substrate instead of graphite. The left panel of this figure strongly suggests an almost complete lack of molecular motion at 100 K aside from an apparent rearrangement period at times under 1 ns; this behavior is also seen in simulations performed at other temperatures below 140 K. At 140 K and above, molecular motion is initiated slowly and then increases in magnitude with increasing temperature, leading to the result seen at the right in Figure 8, which shows oscillations in first-layer composition until roughly 4–4.5 ns into the simulation, at which point the compositions seem to fluctuate about fixed positions. This result also mirrors conclusions from Paper I, in which calculations of root-mean-square displacement of molecules of single-component halomethane films adsorbed on hydroxylated SiO₂ showed little or no motion—either along the surface or into the bulk film—at or below 140 K.

Because of the apparently slow dynamics of first-layer molecules adsorbed on hydroxylated SiO₂ in simulations performed at low temperatures, it was natural to question whether or not the population fractions obtained after long simulation times (sometimes 10 ns or longer) represented a true equilibrium

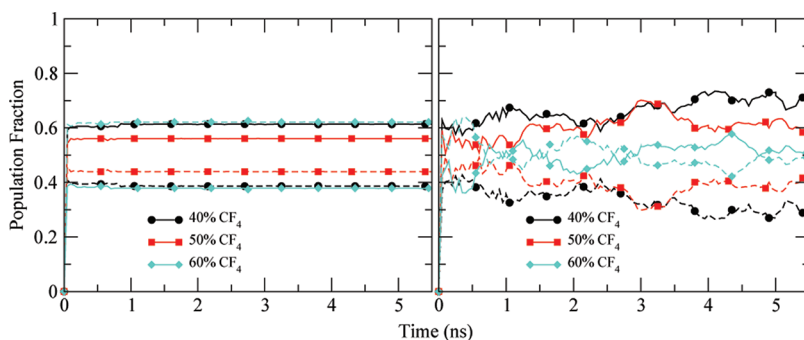


Figure 8. Surface-layer population fractions of CF_4 (dashed curve) and CF_3Br (solid curve) adsorbed on hydroxylated SiO_2 as a function of time for films of differing overall composition at two different temperatures: 100 K (left) and 200 K (right).

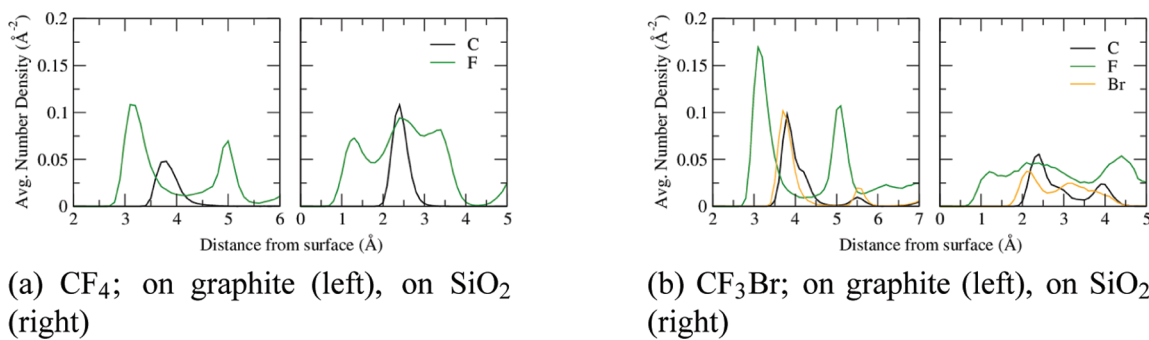


Figure 9. Average number density of a representative case (60% CF_4) at 100 K, separated by atom type for each component molecule.

structure or whether the dynamics were simply too slow to reach such a structure in a reasonable simulation time. To answer this, several low-temperature simulations were continued much longer than originally assumed to reach equilibrium—at the lowest temperatures, simulations were extended by an order of magnitude, and all were extended several times their original run times. Analyses of these much longer simulations did not suggest any change in the population fractions at the surface, and thus we are confident that the data represent reasonable equilibrium structures.

Orientation at Surfaces. One of the questions raised by the average mass density in Figure 1 and by the number densities in Figure 2 and Figure 3 is the nature of the prominent splitting of peaks in the first-layer region—most notable in the average mass density of the first adsorbed layer on graphite and in the number density of the first adsorbed layer on hydroxylated SiO_2 . Such splitting can be best explained by noting the by-atom nature of the average mass density calculation and the 0.1 \AA bin width utilized in both sets of calculations. Together, these factors result in split peaks because of not only preferential positioning of first-layer molecules relative to one another but also preferred orientations relative to the substrate surfaces, which place specific atoms of each molecule in certain locations relative to the surface, with the differences in mass responsible for the mass density profiles seen. This can be confirmed by examining the number density of each molecule type as a function of distance from the surface by decomposing the number density into the contributions from each atom type in each component molecule type. From this calculation, it is possible to determine how, on average, atoms arrange spatially as well as with respect to one another within a surface-layer molecule. The results of this calculation for a representative case are shown in Figure 9.

In Paper I, three basic orientations were suggested for surface-layer CF_4 molecules:

- a “caltrop” orientation in which an F_3 triad rests closest to the surface, with a lone C–F bond pointing normal to the surface (much like a caltrop resting on a flat surface),
- an “edge-down” orientation, in which two of the fluorine atoms are closest to the surface and are roughly the same distance from the surface, and the other fluorine atoms point up and away from the central carbon atom, and
- an “inverted caltrop” orientation which, as the name suggests, refers to a orientation in which a single C–F bond points directly toward the surface, and the remaining F_3 triad points up and away from the central carbon.

It can be quite common to find significant tilting from the ideal basic orientation, at times producing actual orientations that border on two of these classifications; it is even possible to view the “edge-down” orientation simply as a special case of the caltrop orientation in which rotation of the molecule presents two C–F bonds that point away from the surface instead of only one. In this study, however, the edge-down and caltrop orientations are considered distinct, and all three orientations are presented as the basic orientations from which tilting deviations may occur.

In graphs of number density such as those in Figure 9, the most pertinent information can be gained from the area under the density graph, which is proportional to the total number of atoms of a particular type found within the integration region; the average number of atoms of a given type within a given region can be obtained by multiplying the integral of number density by the surface area. The average number density of CF_4 in Figure 9a reveals a single-peak region for carbon atoms, centered around a

distance of roughly 3.75 Å from the substrate, and two well-separated fluorine peaks at 3.15 and 5 Å. Integration over each of the fluorine peaks and the single carbon peak shows that the number of fluorine atoms in the peak region at 3.15 Å is roughly 2.5 times the number of carbon atoms within the carbon peak region, and that the number of fluorine atoms in the second peak region is roughly 1.5 times that of the carbon peak region. This plus the position of the carbon peak, closer to the 3.15 Å fluorine peak, suggests that the preferred orientation for CF_4 on graphite is the caltrop orientation, with a notable minority in the edge-down orientation. This distribution of atoms further suggests that the inverted caltrop is very much a minority contribution, if it is indeed present, as a carbon contribution at greater distance from the surface would be expected. This agrees well with our previous findings for pure CF_4 films on graphite from Paper I.

For CF_4 adsorbed on hydroxylated SiO_2 (Figure 9a), however, the presence of three peaks that are not well differentiated with respect to one another, along with a carbon peak region roughly at the center of the fluorine region, suggests that CF_4 shows no specific preference for orientation near the SiO_2 surface. In this case, the three peaks of the fluorine distribution may possibly suggest a well-mixed contribution from each of the three basic orientations, along with the presence of tilted orientations that prevent fluorine atoms from being seen in specific positions. In essence, the behavior seen is what might be expected of a spherical molecule in that the central atom locates near the center of a region that extends roughly the same distance on either side, which might be expected of the symmetric CF_4 molecule should interaction with the substrate not favor any particular orientation.

In our study of pure halomethane films on graphite and hydroxylated SiO_2 , a rough conclusion was drawn for the orientations of CF_4 based on a similar accounting of the fluorine positions relative to the central carbon position, and the two approaches taken produce similar results. There, an apparent competition existed between edge-down and caltrop orientations, with each in similar numbers—in that case, the edge-down contribution was expected to be slightly larger, whereas in the present binary mixtures, it is the caltrop orientation that is expected to be favored slightly—and with the inverted caltrop orientation well in the minority, if present at all. Thus, to this extent, CF_4 , as part of a binary mixture with polar CF_3Br , appears to exhibit much the same behavior it did in pure-film adsorption with respect to orientation. Our previous analysis also suggested, though, that CF_4 on hydroxylated SiO_2 should orient predominantly in the edge-down orientation. Looking at Figure 9a, the edge-down orientation seems a likely major contributor, although a predominantly edge-down system would be expected to present a fluorine number density along the z -direction with only two major peaks, and integrating those peaks should show larger numbers than the carbon peak. Instead, what is seen is a three-peak distribution, with nearly equal amplitude among all three peaks and significant populations of fluorine between the peaks. This suggests the orientations of CF_4 on the hydroxylated SiO_2 substrate are much more varied than previously assumed for CF_4 within the binary mixture.

Determining the preferred orientations of polar CF_3Br molecules is aided by the asymmetry introduced by the C–Br bond. Monitoring the C–Br bond orientation relative to the substrate surface in Paper I allowed identification of three basic preferred orientations of the CF_3Br molecule, using this bond as the descriptor:

- A “parallel” orientation, in which an F_2 edge rests closest to the substrate surface, with the carbon and bromine atoms just above. In this case, the C–Br bond is oriented parallel to the substrate surface or points slightly toward the substrate ($<10^\circ$, generally, as will be shown), and the remaining C–F bond out and away from the surface.
- A “tripod” orientation, in which the molecule presents the F_3 triad toward the surface as if resting on the three C–F bonds. In this arrangement, the C–Br bond points normal to the surface, away from the interface.
- An “inverted tripod” or “antitripod” orientation, in which the molecule presents the F_3 triad to the bulk film, and the C–Br bond is directed normal to the surface, toward the surface.

As with the CF_4 orientations, significant tilting of the C–Br bond can be seen in all simulations.

Adsorption of CF_3Br on graphite (Figure 9b) shows a two-peak fluorine distribution (also at positions of roughly 3.15 and 5 Å above the surface), with a very minor peak around 6.2 Å. A major carbon peak region can be found at roughly 3.8 Å, similar to CF_4 on graphite, and there is evidence of a very small secondary carbon peak at roughly 5.5 Å above the substrate surface, nearly at the edge of the first layer. Contributions from bromine atoms appear to nearly mirror the distribution of carbon atoms: a major peak at roughly 3.7 Å above the graphite surface, with a small secondary peak at 5.5 Å. The asymmetry introduced by the C–Br bond is convenient in that it suggests rather simply the orientation of the molecule as a whole, and in the case of CF_3Br on graphite, that the bromine atoms appear to predominantly prefer a position almost aligned with the carbon atoms (relative to the surface) suggests that the overwhelmingly favorite orientation features a C–Br bond nearly parallel to the surface or pointing just slightly toward the surface. The larger fluorine distribution close to the surface suggests that the preferred overall orientation features an F_2 edge closest to the surface, a C–Br bond parallel to the surface and slightly further from it, and a singular C–F bond pointing away from the surface. A small contribution from the antitripod orientation is likely the reason for the small carbon peak at 5.5 Å together with the minor fluorine peak at 6.2 Å (the combination of these suggests a small contribution from a CF_3 group near the upper edge of the layer) and may contribute to the bromine peak at 3.7 Å. The secondary bromine peak may also be due to a minority in the tripod orientation, which would place a segment of the bromine distribution much higher in the z -direction, without directly increasing the carbon or fluorine distributions in the same area.

On the hydroxylated SiO_2 substrate, the preferred orientation of the CF_3Br molecule is not nearly as pronounced. The average number density seen in Figure 9b shows atomic positions spread over a much broader region in the z -direction, which partially accounts for the much lower number density amplitude seen in the figure. Integration of the number density over the first-layer region confirms that the correct number of molecules are present. Fluorine atoms in the first layer appear to be more or less distributed evenly, with a moderate peak at 4.4–4.5 Å from the surface, but otherwise without any major features. The existence of a carbon peak from roughly 2 to 2.7 Å along with a bromine peak region slightly lower, at 1.8–2.5 Å, suggests the parallel orientation may be a large contributor for adsorption on SiO_2 , albeit with significant tilting of the C–Br bond toward the surface, noted by the larger difference between the carbon and bromine peak positions. Broad, diffuse secondary peaks in carbon

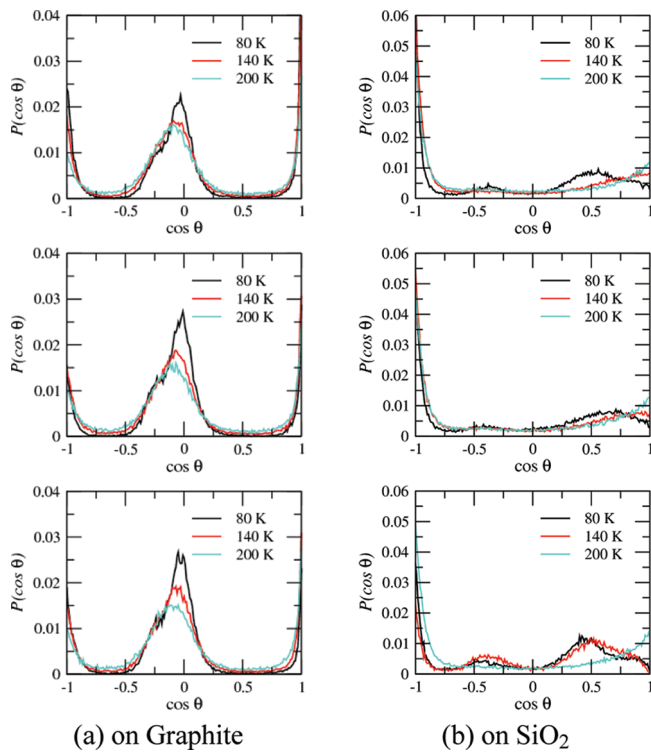


Figure 10. Probability density function estimation for the orientation angle of the C–Br bond in CF_3Br for compositions of 40% CF_4 (top), 50% CF_4 (center), and 60% CF_4 (bottom). Angle θ is measured with respect to the surface normal (positive z -axis).

and bromine make determination of the orientations of minority contributors more difficult in this analysis but are suggestive of sizable contributions from inverted orientations.

The asymmetry of the CF_3Br molecule may be exploited in a different fashion to possibly answer the questions posed by Figure 9b. Calculation of the probability density function for the orientations of C–Br bonds near the surface, relative to the surface normal (positive z -axis), may offer a less position-dependent analysis of orientation. The results of such a calculation, relating the probability of finding a given C–Br bond making an angle θ with the surface normal, are plotted in Figure 10, with the measure of the angle given in terms of its cosine.

Similar to what was found in the previous examination of pure films, in the case of mixed films on graphite, there is a notable peak just below $\cos(\theta) = 0$, which suggests that a significant population of CF_3Br molecules are oriented with the C–Br bond pointed nearly parallel to the surface or slightly toward it (negative cosine values). This peak region does not appear to broaden significantly as the system temperature increases, but the amplitude of the peak region declines, as do the amplitudes of regions near $\cos(\theta) = \pm 1$. Commensurate with this decline in peak amplitudes is an increase in the probability density at values of $\cos(\theta)$ outside of the central peak region. Because values of $\cos(\theta)$ equal to $-1, 0$, and 1 most closely represent, respectively, the antitriple, parallel, and triple orientations, a conclusion to be drawn from this data is that at low temperatures, CF_3Br molecules are most likely to be found in one of the three basic orientations, with significant tilting about the parallel orientation (owing to the width of the central peak region), and that as temperature increases, increasing numbers of molecules will shift

to more random orientations, although a majority will remain essentially in the original basic orientations. Also of note is a shift in central peak position, as a function of increasing temperature, to more negative values of $\cos(\theta)$, which suggests that the basic parallel orientation present at low temperatures becomes slightly more oriented toward the surface as the temperature increases. While the entirety of this central peak region seems to exist over a range of angle values between roughly 70° and 120° , the peak value only shifts from a maximum at 91° at low temperatures to 96° relative to the surface normal; thus, it appears the majority of CF_3Br on graphite prefers orientations that range from nearly parallel (at low temperatures) to only slightly more toward the surface.

However, as noted from the atomic number density in Figure 9, CF_3Br on SiO_2 seems to show only one specific orientation contributing significantly to the first-layer population—at low temperatures, the probability density shows a high, sharp peak at $\cos(\theta) = -1$, suggesting an inverted tripod. This may be related to the secondary carbon peak and the low- z fluorine peak seen in Figure 9b, as this would produce a sizable inverted tripod population. The surface layer of each composition at temperatures at or below 140 K also appears to show a bimodal distribution (apart from the inverted tripod segment) with two low, broad peaks: one at moderately negative values of $\cos(\theta)$, indicating bond vectors pointing toward the surface (angles between 95° and 125° , in line with the prediction of a substantially tilted parallel orientation), and one larger but very broad peak centered around $\cos(\theta)$ values of roughly 0.4 – 0.7 (roughly 45 – 65°), with the central value of this peak varying with film composition but without a clear pattern in such variation. From this, the most likely secondary orientation appears to be a highly tilted tripod orientation, which is also in line with the main carbon peak and low- z fluorine peaks in Figure 9b. As the temperature increases, the bimodal distribution fades in favor of contributions from antitripod molecules, and the smaller low-peak regions shift toward cosine values close to unity, suggesting a shift to tripod orientations, especially those tilted at a smaller angle relative to the surface normal.

CF_3Br adsorbed on graphite in a binary mixture with CF_4 also exhibits similar orientation profiles as it does in single-component films on graphite. In both cases, sizable contributions are made from tripod and antitripod orientations, and similarly large contributions come from molecules in parallel or tilted parallel orientations, with similar ranges of tilt angles (roughly 70 – 120°). Even similar effects of temperature variation may be noted: contributions from the tripod and antitripod orientations decrease in number, the most probable tilt angles—near the peak of the parallel orientation region—shift to slightly larger values and also decrease in number, and the numbers of molecules with orientations outside the basic three increase in number. As with CF_4 on graphite, it appears that CF_3Br on graphite does not note the difference between being in a single-component film or a binary mixture as far as surface orientation is concerned.

On the other hand, orientations appear slightly altered from CF_3Br on hydroxylated SiO_2 depending on whether or not another chemical species is part of the film. In single-component CF_3Br films on hydroxylated SiO_2 , at low temperatures a peak is seen in the range of tilt angles from 150° to 180° , corresponding to antitripod and tilted antitripod configurations, and such a feature is also present with CF_3Br in the mixture. In single-component films, however, CF_3Br in Paper I showed only one other major peak, corresponding to tilt angles of roughly

Table 1. Estimated Binding Energy for Halomethanes on Graphite and Hydroxylated SiO₂

molecule	substrate	orientation	<i>E</i> _{bind} (kcal/mol)
CF ₄	graphite	caltrop	4.63
		edge-down	4.04
CF ₄	SiO ₂	average	4.18
		parallel	6.72
CF ₃ Br	graphite	tripod	4.77
		antitripod	3.66
		parallel	5.29
CF ₃ Br	SiO ₂	tripod	3.96
		antitripod	3.81

10–70°, largely corresponding to a wide array of tilted tripod orientations, and at high temperatures, these two peaks seem to merge into a single, broad peak centered at roughly 100–105°, which would correspond to a more parallel-like orientation, along with notable random contributions at other tilt angles. In CF₃Br within a mixture, however, the tilted tripod contribution seems to shift to larger tilt angles, and the previously mentioned low, broad secondary peak, corresponding to a substantially surface-tilted parallel orientation, emerges. Subsequently, it seems both the intermediate broad peaks merge into antitripod and tripod orientations as temperature increases in the mixture case, which is substantially different from the orientations seen in the single-component study.

Questions about both number density and surface orientation can be related to the energetics of molecular binding to the surface. The binding energy, *E*_{bind}, between a molecule and the substrate can be estimated by

$$E_{\text{bind}} = E_s + E_m - E_{\text{ad}} \quad (1)$$

where *E*_s is the total potential energy of the surface with no adsorbate present, *E*_m is the total potential energy of a single first-layer molecule (in a specified orientation) without the presence of the substrate or other adsorbate molecules, and *E*_{ad} is the total potential energy of the adsorbed first-layer molecule/substrate system. In this case, binding energy estimates were calculated using data from the ends of simulations determined to have reached stable equilibrium states. As molecular orientation was expected to play a role in the binding energy, energy calculations were performed for each orientation suggested by the average number density calculations in Figure 9. The results are shown in Table 1.

The binding energies shown in Table 1 are merely base estimates with which to characterize relative adsorption energetics between different species present in the binary mixtures, as well as to compare the effect of orientation in order to shed light on surface–molecule orientations seen. Nevertheless, the estimates obtained for the binding energies of CF₄ and CF₃Br on graphite appear to agree relatively well with previous estimates gained from simulation^{23,37} and appear reasonable with respect to isosteric heats of adsorption obtained from studies on planar graphite and carbon nanotubes.^{10,11}

What may be gleaned from the estimation of binding energy is that for CF₄ mixtures on graphite, the caltrop and edge-down orientations seem to be nearly equally favored energetically (the caltrop orientation may prevail somewhat), but that both binding energies are significantly lower than the binding energy of CF₃Br in the parallel orientation and are less than or almost

equal to the binding energy of the CF₃Br tripod orientation. This would suggest that the reason for the observed dominance of CF₃Br at the surface of binary mixtures on graphite, as well as the predominance of the parallel orientation of CF₃Br within those mixtures, is the energetic favorability toward CF₃Br physisorption on the graphite surface. It should be noted here that the inverted caltrop orientation of CF₄ was such a small contributor to the overall population to the first adsorbed layer on graphite that it was not observed in the simulations from which binding energy was derived. The CF₃Br antitripod orientation exhibits the lowest calculated binding energy of any species or orientation observed on the graphite substrate and thus is expected to be a minority contributor to surface-layer adsorption, if it is present at all. Such determinations seem to agree well with the analysis of the CF₃Br number density in Figure 9b.

On the hydroxylated SiO₂ surface, however, dominance by one species over another is more muted. From analysis of the average CF₄ number density in Figure 9a, we expected that the orientation of CF₄ on the hydroxylated SiO₂ surface would not play a significant role in the adsorption behavior, and analysis of the surface-layer molecules supported this—specific orientations of CF₄ on this surface were extremely difficult to identify clearly, and as a result, an average behavior for all orientations noted is given in Table 1. As was the case with mixtures on graphite, the most energetically favored adsorption on hydroxylated SiO₂ appears to come from CF₃Br in the parallel orientation; however, the relative value of the binding energy for this orientation, compared to the same molecule and orientation on graphite, is much lower, suggesting a more equal weighting between species on hydroxylated SiO₂, and a reason for finding greater numbers of CF₃Br molecules in different orientations. Here, the difference in binding energy between the parallel and tripod orientations on SiO₂ is on the order of 1 kcal/mol, whereas on graphite, the difference was nearly twice as high. Also notable is the lack of a major binding energy difference between tripod-CF₃Br and antitripod, whereas on graphite, the antitripod orientation exhibited a much lower binding energy and was very much a minority contributor to the surface-layer population. From the average behavior of binding energies for the CF₃Br orientations, it can be shown that the binding energies for CF₄ and CF₃Br on hydroxylated SiO₂ appear quite comparable, suggesting a lack of energetic favorability toward binding and providing a probable reason for the lack of preference for one species or the other on the SiO₂ surface beyond the mixture's initial bulk composition.

Structural Correlations at Surface. While the previous section dealt mostly with investigating the positions and orientations of adsorbate molecules with respect to the substrate surface, another important question to ask is what positions are taken by adsorbate molecules with respect to one another and whether there is any apparent medium- or long-range order in the first adsorbed layer. To this end, an investigation of the positional order of the surface molecules may provide important insight into whether or not the presence of multiple species influences the congregation of adsorbed molecules. From previous analysis, it has been established that the greater majority of surface molecules exist essentially in a slab of single-molecule width, with notable space between the surface layer and the second layer, thus eliminating overlap onto the surface layer from the bulk. Thus, determining the level of positional correlation of the first adsorbed layer may be simplified by treating this layer as a two-dimensional surface, analyzing spatial correlations using the

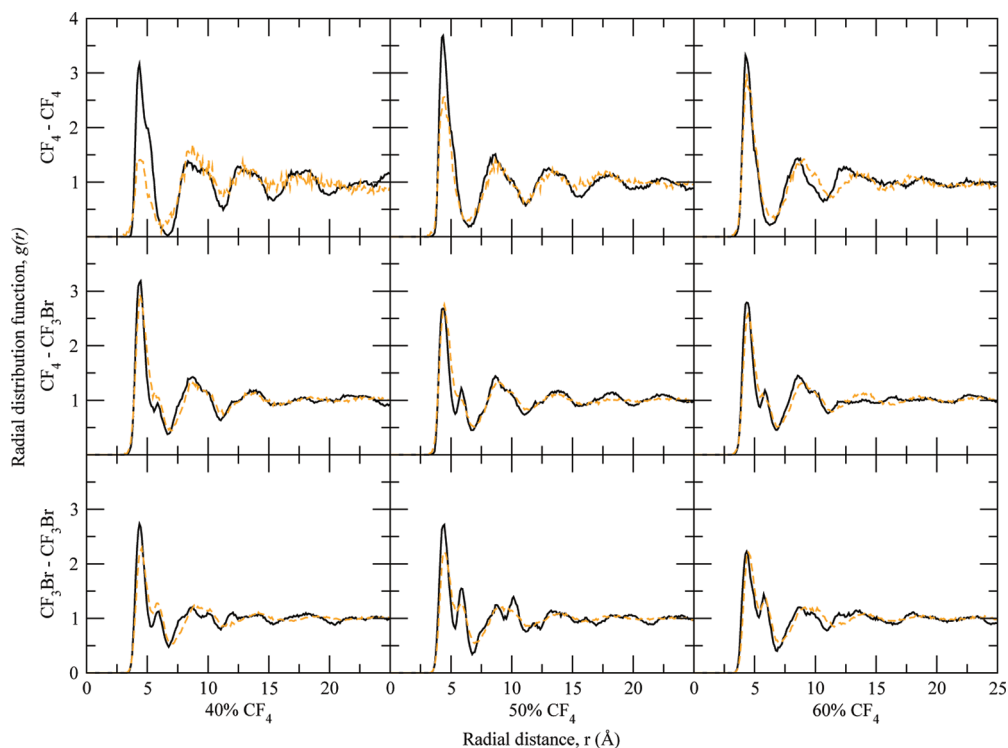


Figure 11. Plots of in-plane radial distribution function, $g(r)$, of layers adsorbed at graphite surface at 80 K (black line, solid) and 160 K (orange line, dashed). For comparison, plots are given comparing across bulk film compositions as well as showing both same-molecule and mixed-molecule contributions.

two-dimensional radial distribution function, $g(r)$,⁹ defined by

$$g(r) = \frac{A}{N^2} \left\langle \sum_i \sum_{j \neq i} \frac{H(r_{ij} - (r - \Delta r/2))H((r + \Delta r/2) - r_{ij})}{2\pi r \Delta r} \right\rangle \quad (2)$$

Here, H is the Heaviside function, A is the surface area of the substrate, N is the total number of molecules within the counting region (in this case, the surface layer), and r_{ij} represents the magnitude of the vector from particle i (a reference particle) to particle in question j . The radial distribution function is constructed by determining the number of molecules within an annulus of radius r and width Δr , summing over each molecule in turn and normalizing with respect to the total number of particles and the number density. The two-dimensional radial distribution function presented offers information regarding the packing of molecules within the surface layer and, subsequently, the number of nearest-neighbor molecules and any positional correlations between molecules. The radial distribution function as presented here uses the position of the central carbon atom as a tag for the molecule as a whole; thus, when future references refer to the radial distribution function as $g(r)$, this should be understood to refer specifically to the carbon–carbon radial distribution function, $g_{cc}(r)$. The use of the carbon atom as a reference is a very reasonable choice for comparing CF_4 molecules, as the symmetry of the molecule means that the position of the carbon atom is coincident with the center of mass of the molecule as a whole, and although asymmetry prevents the same from being true of CF_3Br , the carbon atom is still the pivotal position in the molecule and is seated in relative proximity to the center of mass, compared to intermolecular distances. We therefore feel that the use of the carbon atom as a molecular center is justified.

For binary mixtures, the in-plane radial distribution function for the surface layer can be subdivided into components based on correlations between each species present in the mixture, either as same-species correlations or cross-species correlations. Monitoring of correlations based on difference between same-species and cross-species $g(r)$ may offer possible methods for observing changes in positional order at the substrate surface induced by the presence of different species. Figure 11 shows plots of the in-plane radial distribution function for the surface layer adsorbed on graphite only, with the profile organized by molecular correlation (CF_4-CF_4 , $\text{CF}_4-\text{CF}_3\text{Br}$, and $\text{CF}_3\text{Br}-\text{CF}_3\text{Br}$) as well as bulk composition.

The radial distribution function is particularly useful in relation to quantities involved in molecular packing, as the integral of $\rho g(r)$ (in which rho refers to the mass density) over a radius r gives the number of particles within r of a representative particle. Such information can be used to derive information on local density and packing. By integration over specific peaks, it is possible to determine the average number of nearest-neighbor molecules for a given type of molecule; the integral from $r = 0$ to the first minimum of $g(r)$ is therefore proportional to the number of molecules in the first-nearest-neighbor region, and the existence of numerous peaks suggests a high degree of positional order, as each molecular position can be defined strongly by correlation with other molecules. For instance, examination of the CF_4-CF_4 correlations in Figure 11 for mixtures of 40% CF_4 shows that the number of CF_4 neighbors around a CF_4 molecule is greatly affected by temperature variation within the first-neighbor region, but that the effect of temperature wanes as one moves further away from a given position. Bulk composition also appears to have a limited effect on the radial distribution

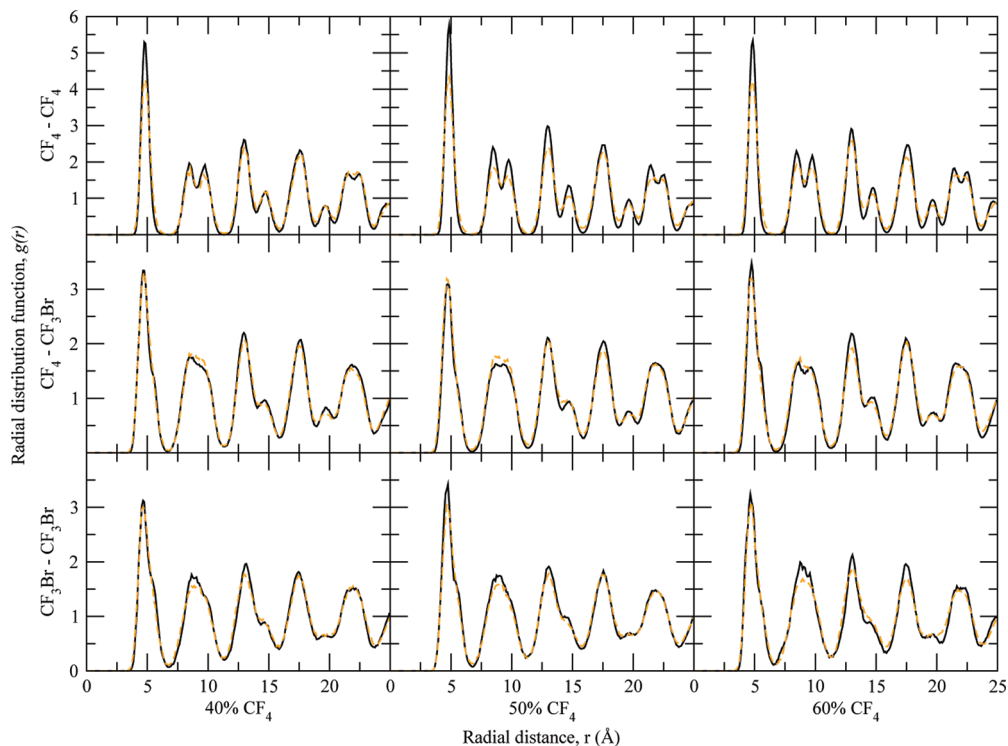


Figure 12. Plots of in-plane radial distribution function, $g(r)$, of layer adsorbed at SiO_2 surface at 80 K (black line, solid) and 160 K (orange line, dashed). For comparison, plots are given comparing across bulk film compositions as well as showing both same-molecule and mixed-molecule contributions.

function beyond the first-peak region; this may suggest that the mixtures are fairly homogeneous and that the majority of information concerning density variation can be taken from first-neighbor estimations, i.e., fluctuations in local density.

It should, therefore, be possible to extract information regarding the evolution of the percent composition of the surface layer as a function of temperature. At low temperatures (80 K, black line in Figure 11), the most noticeable difference between CF_4-CF_4 correlations as a function of bulk composition is in the shape of the first-neighbor peak region in the 40% CF_4 case. While the 40% CF_4 first-peak width appears slightly larger than the first-peak widths in the other cases, the amplitude of the first-peak region is at its lowest for 40% CF_4 , whereas the 50% first-peak region appears to have the highest amplitude, as well as the smallest width. In this sense, then, it appears the areas under the $g(r)$ curves for CF_4-CF_4 for 50% and 60% CF_4 are quite comparable, which suggests the density of CF_4 in the first layer is quite comparable between 50% and 60% CF_4 , and indeed, Figure 6 shows that at 80 K, the percent CF_4 in the first layer is almost equal for the two bulk compositions. Without integrating numerically, it is difficult to ascertain how the surface-layer population of CF_4 in the 40% CF_4 film relates to the other bulk compositions, but the notably lower first-peak amplitude and comparable first-peak width, along with the similar distributions for larger r , suggest that the percentage of CF_4 in the first layer for 40% CF_4 bulk composition at 80 K should be slightly lower than the other cases, which is also the result we see in Figure 6.

At the elevated temperature (160 K), however, there is a dramatic change for the 40% CF_4 film. This film shows a very small first-nearest-neighbor peak, with a noticeable difference in area under the curve compared to not only the 80 K curve at 40%

CF_4 but also much lower area compared to the 50% and 60% CF_4 films, and this seems to very clearly correlate to the surface-layer population fractions seen in Figure 6. In fact, the trend of estimated area under $g(r)$ for CF_4-CF_4 correlations as a function of bulk film composition mirrors the population fractions seen in Figure 6 explicitly: increasing amounts of CF_4 are to be found in the surface layer as the percentage of CF_4 in the bulk increases. A possible caveat to this analysis is considerable noise in the radial distribution function for CF_4-CF_4 correlations at high temperatures and in cases in which CF_4 is the minority component of the bulk. This is most likely a result of the more limited amount of CF_4 molecules in the sample; however, there is little of note beyond the first peak in all of these cases, and there is fair agreement between the low- and high-temperature results beyond the first peak except for the 40% CF_4 film, which shows similarity that is mitigated by the noise level.

Paper I showed that films of pure CF_4 , either adsorbed on graphite or hydroxylated SiO_2 , showed a distinct, clear $g(r)$ structure characteristic of a hexagonal packing arrangement. The radial distribution functions shown in Figure 11 for CF_4-CF_4 correlations, however, exhibit peaks which are broad and do not show the same characteristic positions; the first-nearest-neighbor peak, for the film of 40% CF_4 , shows shoulders that suggest neighbor positions are not as well-defined, and beyond the first-neighbor peak, subsequent peaks tend to merge and decay quickly. It may be expected that the inclusion of an asymmetric, larger polar species should interrupt the orderly packing of CF_4 on the atomically flat graphite surface, but the extent to which CF_3Br induces disorder in the surface packing is not clearly evident.

A notable feature of $g(r)$ involving CF_3Br molecules, and especially in the case of $\text{CF}_3\text{Br}-\text{CF}_3\text{Br}$ correlations, is the minor split peak that appears to be attached to the first-nearest-neighbor peak. This minor peak may be attributable to differences in surface orientation of the polar axis of different molecules; depending on the orientation of the CF_3Br atoms, these differences may manifest as a shoulder or widening of the first-peak region in $g(r)$ if significant numbers of CF_3Br adopt tripod or antitriple arrangements, or it may manifest as a split peak if—as has been suggested by number density, tilt angle, and energetic considerations—the parallel configuration predominates. At low temperatures, the split first peak is notable for both $\text{CF}_3\text{Br}-\text{CF}_3\text{Br}$ correlations and $\text{CF}_4-\text{CF}_3\text{Br}$ correlations at all compositions; at higher temperatures, there is a shift in $\text{CF}_4-\text{CF}_3\text{Br}$ $g(r)$ to a first-peak shoulder, but the split first peak is still noticeable in $g(r)$ for $\text{CF}_3\text{Br}-\text{CF}_3\text{Br}$.

There is little noticeable difference due to temperature change between $\text{CF}_4-\text{CF}_3\text{Br}$ $g(r)$, other than the aforementioned merging of split peaks in the first-neighbor region. Beyond the first-neighbor region, $g(r)$ curves for low and high temperatures are similar in general profile, although films with a high bulk concentration of CF_3Br show a smoothing of peaks at high temperature beyond the first-neighbor region, which may suggest a slight loss of positional order at 160 K. The merging of the split peaks may also be due to greater rotational mobility of CF_3Br molecules at the elevated temperature, increasing the possible placements of the bulky bromine atom. The area under $g(r)$ for $\text{CF}_3\text{Br}-\text{CF}_3\text{Br}$ appears to be relatively similar at 80 K for bulk film compositions of 40% CF_4 and 50% CF_4 , with a slightly larger area under the curve for 40% CF_4 , but the area under $g(r)$ is significantly lower in the case of 60% CF_4 , which is expected from the earlier analysis of composition of the surface layer (Figure 6). Curious is the relative similarity between $g(r)$ values for $\text{CF}_3\text{Br}-\text{CF}_3\text{Br}$ at 160 K, which suggest slight drops in area below the first-neighbor region and possibly the second, but otherwise are nearly identical.

In all cases, $g(r)$ for the binary mixtures on graphite show marked difference from single-component films in that the presence of ordering is significantly decreased in the mixture. In single-component films, $g(r)$ and other analysis suggested CF_4 exhibited orderly hexagonal packing on the surface of graphite, and that while the ordering of CF_3Br was difficult to classify, a moderate degree of packing order was present, based on $g(r)$. In the case of binary mixtures, the rapid decay and featureless regions beyond the first-neighbor regions in each of the analyses in Figure 11 suggests that the mixture exhibits a moderate degree of positional order at best.

The situation changes dramatically when attention shifts from the surface layer on the graphite substrate to the SiO_2 substrate, as is pictured in Figure 12.

Perhaps the most notable effect seen in Figure 12 is how little the radial distribution functions are affected by variation in temperature. Some difference in area below $g(r)$ can be seen in the case of CF_4-CF_4 at all compositions, and minor differences in area are visible for $\text{CF}_3\text{Br}-\text{CF}_3\text{Br}$ correlations; overall, however, there is a large degree of similarity between $g(r)$ at 80 and 160 K at all compositions and in all comparisons. In comparison to $g(r)$ for films on the graphite substrate, this result seems to suggest that the hydroxylated SiO_2 substrate has not only a very significant effect on the packing order of binary mixture films but also a significant effect that severely limits fluctuations in positional order that might arise due to increased mobility as a function of increased temperature.

The CF_4-CF_4 radial distribution is notable in the case of the binary mixture in how much it resembles the radial distribution function for pure CF_4 films on hydroxylated SiO_2 in Paper I. In both cases, $g(r)$ showed a tall, narrow first peak corresponding to a high degree of order in the positioning of first-nearest neighbors, and beyond the initial peak, both show structure that can be correlated with a general hexagonal lattice of particles in two dimensions, i.e., the second-neighbor peak, composed of a split peak of uniform amplitude, which is thought to be a hallmark of the hexagonal lattice. The $\text{CF}_3\text{Br}-\text{CF}_3\text{Br}$ radial distribution function, despite showing significantly more positional disorder than CF_4 , also shows a similar $g(r)$ profile compared to the pure- CF_3Br films on hydroxylated SiO_2 previously studied. One possible implication of the similarities noted here is that one effect of adsorption on the hydroxylated SiO_2 surface is essentially to ignore the presence of two species in a mixture when it comes to surface adsorption and treat all adsorbing species nearly identically.

The mixed contribution, $\text{CF}_4-\text{CF}_3\text{Br}$, in the case of adsorption on SiO_2 has the quality that it appears to be almost an average of the contributions from the CF_4-CF_4 case and the $\text{CF}_3\text{Br}-\text{CF}_3\text{Br}$ cases—the speculation from the previous investigation was that adsorption onto the SiO_2 surface places molecules in a hexagonal “cage” bounded by surface hydrogen bonds and hydroxyl groups, where the effect of adjacent molecules is muted or overwhelmed completely. The investigation of binary mixtures seems to suggest that the adsorption of molecules of the mixture also occurs in such a way as to be largely unaffected by the presence of other molecules and that the surface effects a hexagonal packing arrangement on both components of the mixture. In this sense, while adsorption on graphite presents a binary mixture in which the components interfere with one another and exclude each other based on interactions with the surface, adsorption on hydroxylated SiO_2 seems to present an almost neutral surface that imposes a high degree of positional order, regardless of the halomethane adsorbate with which it interacts.

CONCLUSIONS

In the preceding work, we have used molecular dynamics simulation to examine the adsorption behavior of films of binary mixtures containing varied proportions of two halomethanes, CF_4 and CF_3Br , on graphite and hydroxylated SiO_2 substrates over a range of temperatures from 80 to 200 K in order to determine what effect variation in temperature, adsorbate—substrate and adsorbate—adsorbate interactions, and overall film composition have on film structure, surface arrangement, and orientation. The density of the adsorbed films in all cases shows the influence of both species on the formation of interfaces at both the substrate surface as well as the liquid—vapor interface. In the latter case, number density calculations show the exclusion of CF_3Br at the vapor interface at all temperatures and compositions and on both substrates. Subsequent calculation of the surface tension of each component, an element not commonly available at the temperatures examined, shows clearly that CF_4 has the lower surface tension of the two components, by a margin sufficient to imply that the difference in surface tension dominates the formation of the vapor interface, consistent with the exclusion of CF_3Br noted from the number density.

In studying the interface formed at the substrate surface, density calculations have shown pronounced oscillations near

the surface that correlate with the formation of multiple layers. The most stable of these layers, the first adsorbed layer, exhibits number densities that show the composition of the first adsorbed layer is strongly affected by the interaction between the film and the substrate. In adsorption on the graphite surface, CF_3Br was seen to be the majority component of films at all temperatures studied and at all compositions of the overall film. On hydroxylated SiO_2 , however, neither component was preferred categorically until the temperature exceeded 160 K, at which point the population of CF_3Br began to outpace that of CF_4 again. Below 160 K, however, the composition of the first adsorbed layer mirrored that of the film overall. This difference in first-layer population implies a difference in adsorbate–substrate interaction that necessitates study of the binding energy of the molecules on each substrate.

Calculations of the binding energy for each component suggested not only a difference in preference based on the substrate onto which the mixture was introduced but also a dependence on or preference for specific molecular orientations for each species. On graphite, the most energetically favored molecule was CF_3Br in a “parallel” orientation, in which an F_2Br triad rests closest to the surface, with the C–Br bond making an angle of just over 90° with respect to the surface normal (positive z -axis), thus just below parallel to the surface. Binding energy calculations for CF_4 showed that a “caltrop” orientation, with three fluorine atoms closest to the substrate surface, was preferred by a small margin to orientations with two or one fluorine at the surface; even at this, however, the two most favored orientations for CF_3Br molecules exhibited binding energies on par with or greater than the most preferred CF_4 orientation. For adsorption on hydroxylated SiO_2 , the parallel orientation of CF_3Br was again most favored energetically, but the apparent lack of a preference for any specific CF_4 orientation, coupled with a decreased energetic advantage of parallel CF_3Br and low binding energies for alternate CF_3Br orientations, served as evidence that neither species is preferentially adsorbed on this substrate.

The difference in binding energy between the substrates suggests that in applications in which adsorption of fluoromethanes such as these can be used to reclaim or remove them from waste streams or from atmospheric releases, the hydroxylated SiO_2 surface provides a much more preferable site for adsorption than the graphite surface. However, considerations from Paper I and from the study of the surface structure of hydroxylated SiO_2 in this study suggest the surface characteristics of the SiO_2 substrate may play a greater role in this preferential adsorption than the surface chemistry alone. In such a case, it may be that employment of high-surface-area hydroxylated silicates or silica-containing compounds would provide a much greater potential for removing these gases than would be possible for porous carbon compounds. Indeed, the potential for adsorption of CF_4 using silicon- or silica-containing compounds has been the focus of previous research³⁸ and design development.^{39,40}

Differences in binding energy and preferences (or lack thereof) for either of the species in the mixture were then expected to play a significant role in the lateral arrangement of molecules in the first adsorbed layer. In a previous work²² on adsorption of pure halomethane films on the same substrates, adsorption of CF_4 on graphite showed clear evidence of hexagonal arrangement of molecules, and similar packing was determined for CF_3Br as well, albeit more weakly. In the current study, the combination of the two species seems to have a demonstrable effect in muting the positional order present in the first adsorbed layer, as the film on graphite offered very weak evidence of the

same positional order despite clear orientational order; this positional order was noted to become weaker with increasing temperature. In the case of adsorption on the hydroxylated SiO_2 surface, the previous study saw that the mobility of surface groups allowed hydroxyls at the surface to arrange in an essentially flat, well-ordered zigzag arrangement creating a network of hexagonal cells bounded by hydrogen-bonded hydroxyl groups. This network of cells was seen to impart very strong positional order on adsorbed films, allowing adsorption of one molecule per “cell” and thus forcing the overall first adsorbed layer into a strong hexagonal packing arrangement. In the case of our current binary mixture study, a similar network of hydroxyl groups also forms on the surface, and the surface once again permits only a single molecule to adsorb per cell. In the case of mixtures, however, in line with our binding energy calculations, the surface appears to have no preference for either species, again imposing strong positional order on the first adsorbed layer, in line with the packing arrangements seen previously for pure halomethane films.

■ AUTHOR INFORMATION

Corresponding Author

*E-mail: gml10@zips.uakron.edu (G.M.L.); mtsige@uakron.edu (M.T.).

■ ACKNOWLEDGMENT

The authors gratefully acknowledge the Donors of the American Chemical Society Petroleum Research Fund Grant No. PRF# 47785-G6 and NSF Grant No. DMR0847580 for support of this research.

■ REFERENCES

- (1) Kjaer, K.; Nielsen, M.; Bohr, J.; Lauter, H. J.; McTague, J. P. *Phys. Rev. B* **1982**, *26*, 5168–5174.
- (2) Faßbender, S.; Enderle, M.; Knorr, K.; Noh, J. D.; Rieger, H. *Phys. Rev. B* **2002**, *65*, 165411.
- (3) Flenner, E.; Etters, R. D. *Phys. Rev. B* **2006**, *73*, 125419.
- (4) Zhang, Q. M.; Kim, H. K.; Chan, M. H. W. *Phys. Rev. B* **1986**, *34*, 2056–2059.
- (5) Nagler, S. E.; Dutta, P.; Sinha, S. K.; Horn, P. M.; Moncton, D. E. *Phys. Rev. B* **1989**, *39*, 2826–2829.
- (6) Migone, A. D.; Li, Z. R.; Chan, M. H. W. *Phys. Rev. Lett.* **1984**, *53*, 810–813.
- (7) Hopkins, T. A.; Boyd, D. A.; Xia, Y.; Shifflett, G. M.; Hess, F. M.; Hess, G. B. *J. Chem. Phys.* **2008**, *128*, 154714.
- (8) Nham, H. S.; Drir, M.; Hess, G. B. *Phys. Rev. B* **1987**, *35*, 3675–3678.
- (9) Pinches, M. R. S.; Tildesley, D. J. *Surf. Sci.* **1996**, *367*, 177–195.
- (10) Heroux, L.; Krungleviciute, V.; Calbi, M. M.; Migone, A. D. *J. Phys. Chem. B* **2006**, *110*, 12597–12602.
- (11) Muris, M.; Dupont-Pavlovsky, N.; Bienfait, M.; Zeppenfeld, P. *Surf. Sci.* **2001**, *492*, 67–74.
- (12) Talapatra, S.; Krungleviciute, V.; Migone, A. D. *Phys. Rev. Lett.* **2002**, *89*, 246106.
- (13) Gatica, S. M.; Bojan, M. J.; Stan, G.; Cole, M. W. *J. Chem. Phys.* **2001**, *114*, 3765–3769.
- (14) Stan, G.; Gatica, S. M.; Boninsegna, M.; Curtarolo, S.; Cole, M. W. *Am. J. Phys.* **1999**, *67*, 1170–1176.
- (15) Simonyan, V. V.; Johnson, J. K.; Kuznetsova, A.; Yates, J. T., Jr. *J. Chem. Phys.* **2001**, *114*, 4180–4185.
- (16) Calbi, M. M.; Gatica, S. M.; Bojan, M. J.; Cole, M. W. *J. Chem. Phys.* **2001**, *115*, 9975–9981.
- (17) Müller, E. A. *Environ. Sci. Technol.* **2005**, *39*, 8736–8741.

- (18) Plaza, M. G.; Pevida, C.; Arenillas, A.; Rubiera, F.; Pis, J. J. *Fuel* **2007**, *86*, 2204–2212.
- (19) Cavenati, S.; Grande, C. A.; Rodrigues, A. E. *Chem. Eng. Sci.* **2006**, *61*, 3893–3906.
- (20) Takamura, Y.; Narita, S.; Aoki, J.; Hironaka, S.; Uchida, S. *Sep. Purif. Technol.* **2001**, *24*, 519–528.
- (21) Kowalczyk, P.; Holyst, R. *Environ. Sci. Technol.* **2008**, *42*, 2931–2936.
- (22) Leuty, G. M.; Tsige, M. *J. Phys. Chem. B* **2010**, *114*, 13970–13981.
- (23) Hammond, W. R.; Mahanti, S. D. *Surf. Sci.* **1990**, *234*, 308–314.
- (24) Gay, J.-M.; Suzanne, J.; Pepe, G.; Meichel, T. *Surf. Sci.* **1988**, *204*, 69–97.
- (25) Morishige, K.; Komura, T. *Langmuir* **1998**, *14*, 4887–4890.
- (26) Knorr, K. *Phys. Rep.* **1992**, *214*, 113–157.
- (27) Knorr, K.; Fassbender, S.; Warken, A.; Arndt, D. *J. Low Temp. Phys.* **1998**, *111*, 339–348.
- (28) Bruch, L. W. *J. Phys. Chem. C* **2009**, *113*, 17399–17406.
- (29) Thomas, P.; Velazquez, D.; Hess, G. B. *J. Chem. Phys.* **2011**, *134*, 114702.
- (30) Watkins, E. K.; Jorgensen, W. L. *J. Phys. Chem.* **2001**, *105*, 4118–4125.
- (31) Plimpton, S. *J. J. Comput. Phys.* **1995**, *117*, 1–19; may be found at lammps.sandia.gov.
- (32) Lobo, L. Q.; Staveley, L. A. K. *Cryogenics* **1979**, *19*, 335–338.
- (33) Kudchadker, A. P.; Kudchadker, S. A.; Shukla, R. P.; Patnaik, P. R. *J. Phys. Chem. Ref. Data* **1979**, *8*, 499–517.
- (34) Tsige, M.; Grest, G. *J. Phys. Chem. C* **2008**, *112*, 5029–5035.
- (35) Soares, V. A. M.; de J., V. S.; Almeida, B.; McClure, I. A.; Higgins, R. A. *Fluid Phase Equilib.* **1986**, *32*, 9–16.
- (36) Rathjen, W.; Straub, J. *Proc. 7th Symp. Thermophys. Prop.* **1977**, 839–850.
- (37) Andersson, M. B.; Pettersson, J. B. C.; Marković, N. *Surf. Sci.* **1997**, *384*, L880–L885.
- (38) Heuchel, M.; Snurr, R. Q.; Buss, E. *Langmuir* **1997**, *13*, 6795–6804.
- (39) Li, Y.-E. Separation of CF_4 and C_2F_6 from a Perfluorocompound Mixture. U.S. Patent 6,187,077 B1, Feb. 13, 2001.
- (40) Tamhankar, S. S.; Ramachandran, R.; Biilow, M.; Galica, T. R. Removal of Perfluorocarbons from Gas Streams. U.S. Patent 5,417,742, May 23, 1995.